IET Renewable Power Generation

Special Issue Call for Papers

Be Seen. Be Cited.
Submit your work to a new IET special issue

Connect with researchers and experts in your field and share knowledge.

Be part of the latest research trends, faster.

Read more

The Institution of Engineering and Technology

Received: 13 June 2022 | Revised: 18 November 2022 | Accepted: 23 December 2022

IET Renewable Power Generation

DOI: 10.1049/rpg2.12676

The Institution of Engineering and Technology WILEY

ORIGINAL RESEARCH

Grid interaction of multi-VSC systems for renewable energy integration

Fatemeh Ahmadloo | **Sahar Pirooz Azad**

Department of Electrical and Computer Engineering, University of Waterloo, Waterloo, Canada

Correspondence
Sahar Pirooz Azad, Department of Electrical and Computer Engineering, University of Waterloo, Waterloo, Canada.
Email: sahar.azad@uwaterloo.ca

Funding information
Natural Sciences and Engineering Research Council of Canada

Abstract

Integration of converter-interfaced renewable energy sources (RESs) into the power system and the transfer of power from RESs to remote load centres over high-voltage direct current (HVDC) lines may require connecting multiple voltage-sourced converters (VSCs) to a common alternating current (AC) system. Because of this connection, control loops of various converters will interact through the AC grid, leading to instability and an undesirable transient response. This paper focuses on the system-level integration of multi-VSC systems for the integration of RESs. μ analysis is used to determine under which control modes the independently stabilized VSCs connected to a common AC system ensure the multi-VSC system stability. Furthermore, a sufficient criterion is proposed for the design of the converters' outer control loops independently to ensure the stability of the interconnected multi-VSC system. For cases of severe interactions, where the interconnected multi-VSC system may become unstable even if individual VSCs are stable, a joint controller design for converters is proposed to stabilize the multi-VSC system. The interaction analysis indicates that employing AC voltage control mode by all the converters causes the highest interaction level, and having more converters in reactive power control mode reduces the impact of interactions on the interconnected system stability.

1 | INTRODUCTION

In line with two goals of the United Nations, i.e. providing affordable and clean energy as well as combating climate change, various converter-interfaced renewable energy sources (RESs) are being integrated into the power system. Furthermore, the transfer of renewable power generated by converter-interfaced RESs such as offshore wind farms to remote load centres may require the use of DC lines, which are connected to the AC grid via voltage-sourced converters (VSCs). The connection of VSCs to the grid for the integration of RESs and power transfer over long distances demand coordination at the system level to prevent any unwanted interactions among the converters.

In large-scale power systems with high integration of RESs, multiple VSCs may be connected to a shared point of common coupling (PCC), causing the adjacent converters to interact with one another through their PCCs and cause instability and an undesirable transient response [1, 2]. Although the control loop interactions might happen among the control loops of one single VSC [3–10], the interactions among the control loops of several converters, which will be called external control loop interactions, will hinder the integration of large-scale RESs into the AC grid and will be the focus of this paper.

A VSC usually includes three main control loops in the direct quadrature (dq)-frame: a d-axis control loop, a q-axis control loop, and a phase-locked loop (PLL). Depending on the VSC's operating mode (control mode), the d-axis control loop can regulate either the DC voltage or active power, and the q-axis control loop may regulate the AC voltage or reactive power [11]. Although there are several control loops in a VSC, the literature does not pay specific attention to the impact of VSCs' control modes on the external control loop interactions [1, 2, 12–17].

Specific sets of control modes have been selected for external control loop interaction studies in the existing literature. The DC voltage/AC voltage control mode is considered in [1] for all VSCs, while the inner current loops are neglected. In [1], the interaction of each VSC with the adjacent VSC is modelled by a

transfer function, and Bode diagrams are employed to study the impact of the AC system short circuit ratio (SCR) and changes in the active power of adjacent VSCs on the interactions and consequently on system stability. The interaction analysis in [2] is based on a comparison of the stability regions of individual and interconnected VSCs, but only the DC voltage control loop is considered, and the dynamics of the PLL and the q-axis outer control loop are ignored. [12] attempts to identify the VSC control mode that results in maximum interactions between a VSC and a STATCOM by using relative gain array (RGA) analysis. The studies provided in [12] are not comprehensive as the impact of the *d*-axis control mode on interactions is not considered, and the RGA analysis has only been used to study the interactions among control loops under the steady-state condition and for a specific control mode. Ref.[18] utilizes RGA to find the frequency at which the maximum interactions occur among converters connected to a shared DC system. This frequency is later used to obtain weighting functions for an H_∞ controller design. Interactions among PLLs of multiple VSCs sharing the same PCC are studied in [13, 14]. By considering VSCs as ideal current sources and neglecting the *d*-axis and *q*-axis control loops, [13, 14] examine the impact of interactions between PLLs on stability using the output impedance of VSCs. In [15, 16], interactions between a grid-following and a grid-forming VSC are studied. A robust stability margin with respect to system parametric uncertainties is defined in [15] using μ analysis, and an eigenvalue analysis is employed in [16] to illustrate the impact of connecting VSCs with different control philosophies to the same PCC on system stability. Neither the converters' controller nor the control mode is the focus in [15, 16]; thus, the outer control loops of the grid-following VSC are not involved in the analysis.

The limitations associated with the existing interaction studies can be summarized as follows:

(i) The impact of converters' control mode on the interactions is not explored, and the studies are performed considering a specific set of control modes for each converter. Although the control mode may not be a design choice for any legal or operational reasons, the impact of control modes on the interactions is of high importance as it can facilitate the design of converters' controllers to reduce the interactions and improve system stability.
(ii) The outer control loops and consequently, various control modes of converters are neglected in several interaction studies. This is because the focus of such studies is on identifying system parameters impacting the interactions.
(iii) The existing studies about the impact of controller design on external control loop interactions are limited to the study of overall system eigenvalue locus as the controller gains change. The findings of these studies cannot be applied to the individual controller design of converters such that the interconnected system is stabilized as well. Making a connection between tuning the controllers of individual and interconnected VSCs to stabilize the multi-VSC system is missing from these studies.

In this paper, the interactions are defined as deviations in the response of converters when they are connected to a shared AC system and when they are isolated. Considering this definition, this paper follows the study initiated in [19] and achieves two main objectives: (i) to identify the set of control modes for which the stability of individual VSCs can ensure a system level stability and (ii) to provide a sufficient stability criterion for designing the converter controllers independently such that the multi-VSC system, in the presence of interactions, is stabilized as well. To do so, a stability formulation is provided that relates the stability of the interconnected multi-VSC system to that of the independent VSCs. Then, μ analysis is used to study whether and under which control modes the independently stabilized VSCs connected to a shared AC system stabilize the multi-VSC system. This set of control modes creates the least disruptive impact on the multi-VSC system's stability. Finally, certain recommendations are provided about the design of converters' controllers to reduce the negative impact of interactions on the multi-VSC system's stability.

The main contributions of this paper are as follows:

(i) The impact of control modes of converters on external control loop interactions is studied using μ analysis, and the set of control modes causing the highest and lowest interaction levels are identified.
(ii) In contrast to the existing literature, in this paper, all possible control modes of a grid-following VSC and the full dynamics of inner and outer control loops as well as PLL are considered in the interaction analysis.
(iii) A sufficient stability criterion is proposed to perform an independent design of VSC's controllers that stabilizes the multi-VSC system as well.
(iv) For the set of control modes causing the largest interactions, a joint design for controllers of VSCs is recommended to reduce the negative impacts of interactions on multi-VSC system stability.
(v) The approach taken in this paper directly connects the stability of independent VSCs to that of the interconnected multi-VSC system, providing a new perspective to interaction analysis and mitigation. Although μ analysis has already been used in the literature for robust stability analysis, it is used for interaction analysis for the first time in this paper. This tool is advantageous not only in the control design of multiple VSCs whose simultaneous design is not possible but also when re-tuning of adjacent converter controllers without impacting the entire system stability is required.

2 | MODELLING OF VSCs CONNECTED TO A SHARED PCC

In this section, the state-space and transfer function models of multiple VSCs connected to a shared PCC are presented in the dq-frame. The state-space model is presented to reveal the

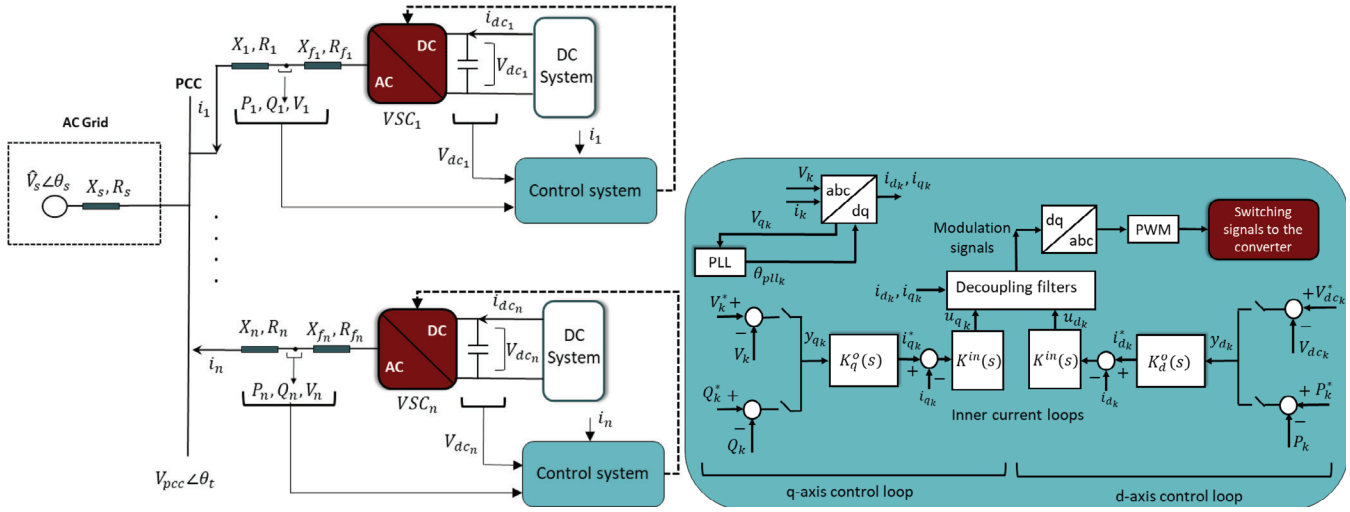

FIGURE 1 (a) Schematic diagram of multiple VSCs having a connection at the AC side and (b) each VSC's control loops

TABLE 1 Parameters of the test system [20]

Quantity	Value	Description
P	200 MW	Active power of each VSC
V_{dc}	400 KV	DC voltage
V_s	230 KV	AC grid RMS voltage
f	60	Frequency
L	0.0291 H	Transformer+ transmission line inductance
L_f	0.0725 H	Filter inductance
C_{dc}	300 μF	DC side capacitance
K_p^{pll}, K_I^{pll}	50, 716	PLL controller gains

mechanism of interactions, and the transfer function model is used in Section 3 for interaction analysis. For further clarity, indices d and q refer to the d and q components of a variable, and "$\vec{\ }$" and "$\sim$" respectively denote the space phasor and the small-signal representation of a variable.

Figure 1a shows the schematic of a multi-VSC system, and Figure 1b shows the control system of each VSC, where the control loops are in the cascaded inner-outer scheme. Because the focus of this work is control loop interactions, the AC side of each VSC is modelled only as an impedance, and all the elements behind the PCC are modelled by a voltage source behind an impedance [1, 15]. The parameters of the converters, which are needed for numerical illustrations, are given in Table 1. Using the space-phasor representation of the current–voltage dynamics at the AC side

$$L_s \frac{\mathrm{d}(\vec{i}_1 + \cdots + \vec{i}_n)}{\mathrm{d}t} = -R_s(\vec{i}_1 + \cdots + \vec{i}_n) + \vec{V}_{\mathrm{pcc}} - \hat{V}_s e^{j\theta_s} \quad (1)$$

where $\hat{V}_s$, θ_s, L_s, and R_s are respectively the voltage magnitude, voltage phase, inductance, and resistance of the AC system, $\hat{V}_{\mathrm{pcc}}$ is the magnitude of the voltage at the PCC, and i_k is the AC line current of VSC_k given by

$$\vec{i}_k = (i_{d_k} + j i_{q_k}) e^{j\theta_{pll_k}}; \quad k = \{1, 2, \ldots n\}, \quad (2)$$

where θ_{pll_k} is the reference frame angle provided by the PLL of VSC_k. The dedicated PLL of each VSC aligns its q-axis with the voltage at the corresponding converter terminal (V_k in Figure 1). Combining (1) and (2) with the voltage–current relationship at the converters' terminals and considering the decoupling filters [11], the dq-components of the voltage at the AC terminal of VSC_k are given by

$$\begin{aligned} V_{d_k} = & \left[R_s + R_k - \frac{X_s + X_k}{X_{f_k}} R_{f_k}\right] i_{d_k} + \frac{X_s + X_k}{X_{f_k}} u_{d_k} \\ & - [X_k + X_s] i_{q_k} + \hat{V}_s \cos\theta_{ps_k} \\ & + \underbrace{\sum_{j=1, j\neq k}^{n} \left[\left[\left(R_s - R_{f_j}\frac{X_s}{X_{f_j}}\right) i_{d_j} + \frac{X_s}{X_{f_j}} u_{d_j} - X_s i_{q_j}\right] \cos\theta_{p_k p_j}\right.}_{\text{Couplings}} \\ & + \underbrace{\left.\left[\left(R_s - R_{f_j}\frac{X_s}{X_{f_j}}\right) i_{q_j} + \frac{X_s}{X_{f_j}} u_{q_j} + X_s i_{d_j}\right] \sin\theta_{p_k p_j}\right]}_{\text{Couplings}}, \end{aligned} \quad (3)$$

$$V_{q_k} = \left[R_s + R_k - \frac{X_s + X_k}{X_{f_k}} R_{f_k}\right] i_{q_k} + \frac{X_s + X_k}{X_{f_k}} u_{q_k} + [X_k + X_s] i_{d_k} - \hat{V}_s sin\theta_{ps_k} \underbrace{- \sum_{j=1, j\neq k}^{n} \left[\left[\left(R_s - R_{f_j}\frac{X_s}{X_{f_j}}\right) i_{d_j} + \frac{X_s}{X_{f_j}} u_{d_j} - X_s i_{q_j}\right] sin\theta_{p_k p_j}\right.}_{\text{Couplings}} \underbrace{\left. + \left[\left(R_s - R_{f_j}\frac{X_s}{X_{f_j}}\right) i_{q_j} + \frac{X_s}{X_{f_j}} u_{q_j} + X_s i_{d_j}\right] cos\theta_{p_k p_j}\right]}_{\text{Couplings}}, \tag{4}$$

where R_f and X_f are respectively, the resistance and reactance of each VSC's terminal filter, R and X represent the total resistance and reactance of the transformer and the transmission line connecting each VSC to the PCC, u_d and u_q are the control signals, $\theta_{ps_j} = \theta_{pll_j} - \theta_s$, and $\theta_{p_j p_k} = \theta_{pll_j} - \theta_{pll_k}$. The parameters of any other desired topology at the AC side can be embedded in the above-mentioned impedances.

Coupling terms identified in (3) and (4) are associated with the variables of adjacent VSCs. Thus, if the VSCs do not have a connection at the AC side, these terms become zero, and each VSC operates as if it is the sole converter connected to the AC system, and consequently, there will be no interactions among the VSCs. In the rest of the paper, the term "*uncoupled*" dynamics refers to Equations (3) and (4) without the coupling terms, and the multi-VSC system, in this case, is an interaction-free system (IFSYS). The term "*coupled*" dynamics refers to (3) and (4) in the presence of coupling terms, and the multi-VSC system, in this case, is an interconnected system (INSYS).

Considering (3) and (4) as well as the active power, reactive power, and DC-link voltage equations [11] of each VSC in Figure 1, the small-signal dynamics of the system can be described by the multi-input multi-output state-space model of

$$\dot{x}_k = A_{kk} x_k + \sum_{j=1, j\neq k}^{n} [A_{kj} x_j + B_{kj} u_j], \tag{5}$$

$$y_k = C_{kk} x_k + \sum_{j=1, j\neq k}^{n} [C_{kj} x_j + D_{kj} u_j], \tag{6}$$

where $x_k = [\tilde{i}_{d_k}, \tilde{V}_{dc_k}, \tilde{i}_{q_k}, \tilde{\theta}_{pll_k}, \tilde{x}_{pll_k}]^T$, $\tilde{x}_{pll_k}$ is the internal state of PLL, $u_k = [u_{d_k}, u_{q_k}]^T$ is the converter control input, and $y_k = [y_{d_k}, y_{q_k}]^T$ is the converter control output, $k \in \{1, , \ldots, n\}$. The d-axis control output (y_d) can be either the DC voltage or active power, and the q-axis control output (y_q) shows the voltage or reactive power of the AC terminal, depending on the VSC's control mode. It should be noted that (5) and (6) provide the full small-signal dynamics of the multi-VSC system with the fast current dynamics and PLL included. As the objective of the paper is to study the impact of control modes on the external control loop interactions, the PLL is not modelled separately and is embedded in (5) and (6). Furthermore, in (5) and (6), no perturbation from the DC side is considered because the aim is to study the interactions among the VSCs sharing a PCC, not those sharing a DC system.

Based on the state-space model in (5) and (6), the state variables of each VSC are impacted not only by its state variables and control inputs but also by those of the adjacent converters, resulting in the coupled transfer function matrix of

$$G(s) = \begin{bmatrix} G_{11}(s) & \ldots. & G_{1n}(s) \\ G_{21}(s) & \ldots & G_{2n}(s) \\ \ldots & \ldots & \ldots \\ G_{n1}(s) & \ldots & G_{nn}(s) \end{bmatrix}_{2n\times 2n}, \tag{7}$$

where $G_{ij}(s)$ is a 2×2 transfer function matrix. By neglecting the coupling dynamics in (3) and (4) and consequently neglecting the off-diagonal matrices $A_{kj}, B_{kj}, C_{kj}, D_{kj}$ in (5) and (6), the IFSYS of VSCs can be described by the uncoupled transfer function matrix

$$\bar{G}(s) = \begin{bmatrix} \bar{G}_{11}(s) & 0 & \ldots & 0 \\ 0 & \bar{G}_{22}(s) & 0 & \ldots \\ \ldots & \ldots & \ldots & \\ 0 & \ldots & 0 & \bar{G}_{nn}(s) \end{bmatrix}_{2n\times 2n}, \tag{8}$$

where $\bar{G}_{kk}(s)$ is different from $G_{kk}(s)$ due to the off-diagonal matrices $A_{kj}, B_{kj}, C_{kj}, D_{kj}$ in (5) and (6).

3 | INTERACTION ANALYSIS

In this section, μ analysis is introduced as the method of analysis to study the impact of the control mode on external interactions and to identify the control modes for which stabilizing the IFSYS of VSCs ensures the stability of the INSYS of VSCs.

3.1 | Interaction impact on system small-signal stability

To illustrate the impact of interactions on system stability, the dominant eigenvalues of the INSYS of three VSCs are presented in Figure 2. In Figure 2, SCR = 1.3 and all VSCs operate in DC voltage/AC voltage control mode. The VSCs are independently stabilized, and therefore, the IFSYS is stable. The set of outer controllers is $K^o_{d_k} = 3.13 + \frac{5.91}{s}$, $K^o_{q_k} = 0.0011 + \frac{2.73}{s}$, $k \in \{1, 2, 3\}$ (similar for all three VSCs). These controllers are obtained for each VSC independent of the others such that the outer control loops are at least ten times slower than the inner loops (with the time constant of 2 ms), and the maximum overshoot is 20%. The time-domain step response of VSC_1 is presented in Figure 2b to show the dynamic response of the independently designed VSCs. Based on Figure 2a, although the IFSYS is stable and has a satisfactory dynamic response,

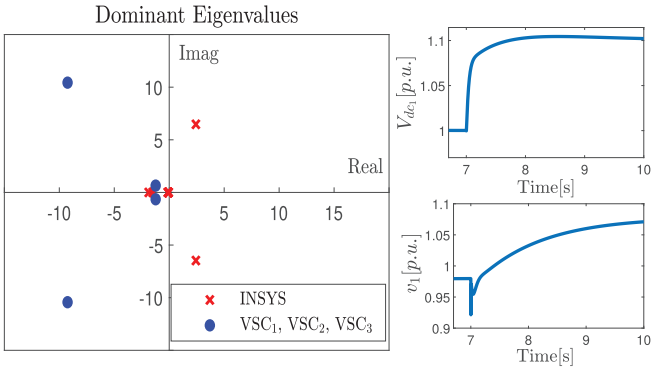

FIGURE 2 (a) Dominant system eigenvalues for a certain set of controller parameters and (b) time-domain response of VSC_1

TABLE 2 Various sets of control modes in a 3-VSC system

Control mode No.	Control outputs	Control mode No.	Control outputs
CN_{11}	$y_1 = [V_{dc_1}, v_1]$	CN_{21}	$y_1 = [P_1, v_1]$
	$y_2 = [V_{dc_2}, v_2]$		$y_2 = [P_2, v_2]$
	$y_3 = [V_{dc_3}, v_3]$		$y_3 = [P_3, v_3]$
CN_{12}	$y_1 = [V_{dc_1}, v_1]$	CN_{22}	$y_1 = [P_1, v_1]$
	$y_2 = [V_{dc_2}, v_2]$		$y_2 = [P_2, v_2]$
	$y_3 = [V_{dc_3}, Q_3]$		$y_3 = [P_3, Q_3]$
CN_{13}	$y_1 = [V_{dc_1}, v_1]$	CN_{23}	$y_1 = [P_1, v_1]$
	$y_2 = [V_{dc_2}, Q_2]$		$y_2 = [P_2, Q_2]$
	$y_3 = [V_{dc_3}, Q_3]$		$y_3 = [P_3, Q_3]$
CN_{14}	$y_1 = [V_{dc_1}, Q_1]$	CN_{24}	$y_1 = [P_1, Q_1]$
	$y_2 = [V_{dc_2}, Q_2]$		$y_2 = [P_2, Q_2]$
	$y_3 = [V_{dc_3}, Q_3]$		$y_3 = [P_3, Q_3]$

the locations of the eigenvalues indicate that the INSYS of these three VSCs is unstable.

For clarity and simplicity of the analysis in the rest of the paper, Table 2 presents the various possible combinations of control modes for a 3-VSC system, as a specific case of a multi-VSC system. Since the parameters of the converters are similar and to prevent redundancy, not all the possible permutations are included. The "control mode No." will be used later to refer to each set of control modes.

3.2 | Method of analysis

Figure 3a shows the VSCs' combined inner and outer controllers, which are designed independently for each VSC such that the IFSYS is stable and well-behaved, and Figure 3b shows the employment of the independently designed controllers in the INSYS of three VSCs. The combined inner–outer

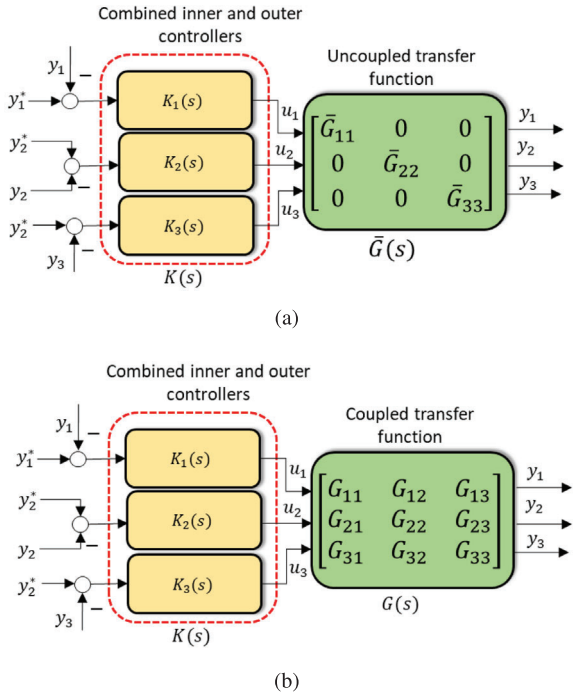

FIGURE 3 (a) Independently designed controllers of the IFSYS and (b) INSYS with the independently designed controllers

controllers of VSC_k is described by

$$\underbrace{K_k(s)}_{2\times2} = \underbrace{\frac{K_k^{in}(s)}{1 + K_k^{in}(s)\left(\frac{1}{L_{f_k}s + R_{f_k}}\right)}}_{K_k^{in,cl}(s)} \underbrace{K_k^{o}(s)}_{2\times2}; k \in \{1, \dots, n\}, \quad (9)$$

where $K_k^{in}(s)$ is the inner controller and $K_k^{o}(s)$ is the outer controller. The controller of the multi-VSC system is given by

$$K(s) = diag(\left[K_1(s), \quad \dots \quad , K_n(s)\right])_{2n\times2n}.$$

For two systems with the transfer functions $G(s)$ and $\bar{G}(s)$ and controller $K(s)$, the characteristic polynomials $det(I + GK)$ and $det(I + \bar{G}K)$, respectively, can be used to study system stability. The relationship between the two characteristic polynomials is

$$det(I + GK) = det(I + \bar{G}K)det(I + E\bar{T}), \quad (10)$$

where E is the relative difference between the coupled and uncoupled transfer function matrices, defined by [21]

$$E = (G - \bar{G})\bar{G}^{-1}, \quad (11)$$

and $\bar{T}$ is the complementary sensitivity function such that $\bar{T} = I - (I + \bar{G}K)^{-1}$. According to (10) and assuming that $\bar{T}$ is stable, $det(I + GK)$ will have all its roots in the open left-half plane (LHP) if and only if $det(I + E\bar{T})$ has all its roots in the LHP [21].

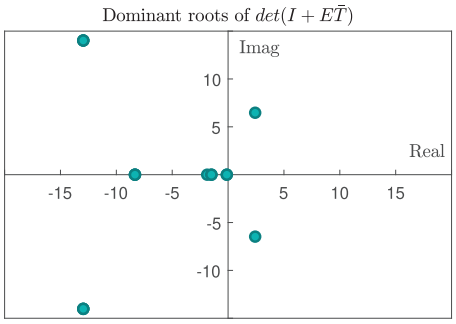

FIGURE 4 Dominant roots of $det\,(I + E\bar{T})$ for the set of controller parameters used in Figure 2.

The term $det\,(I + E\bar{T})$ in (10) indicates how the characteristic polynomial of the IFSYS changes with interactions to form the characteristic polynomial of the INSYS. Therefore, as long as the interactions among the converters do not result in the roots of $det\,(I + E\bar{T})$ leaving the LHP, IFSYS's stability ensures INSYS's stability. Figure 4 shows the roots of $det\,(I + E\bar{T})$ for the set of controller parameters used in Section 3. A. As some of the roots of $det\,(I + E\bar{T})$ are not located in the LHP, the IFSYS stability does not result in the stability of INSYS, which was also shown in Figure 2a.

To have all the roots of $det\,(I + E\bar{T})$ in the LHP, the Nyquist plot of $det\,(I + E\bar{T})$ must not encircle the origin, which leads to the sufficient stability condition of

$$\rho(E\bar{T}(j\omega)) < 1 \quad \forall\omega, \tag{12}$$

where ρ is the spectral radius [21]. Equation (12) is a sufficient condition ensuring INSYS stability in the presence of interactions, when IFSYS is stable. A weaker sufficient condition for INSYS stability based on (12) is to have

$$\bar{\sigma}(\bar{T}(j\omega)) < \mu(E(j\omega))^{-1} \quad \forall\omega, \tag{13}$$

where $\bar{\sigma}$ is the maximum singular value [21]. μ is the structured singular value defined by

$$\mu(E) = \frac{1}{\min_{\Delta}\{\bar{\sigma}(\Delta)\,|\,\det(I - E\Delta) = 0\}}, \tag{14}$$

where the structured uncertainty Δ has a block-diagonal structure similar to the structure of $\bar{T}$ [21]. $\mu(E)$ can be computed for any given E and by searching through stable perturbations Δ with a similar structure to $\bar{T}$ and finding the reciprocal of the smallest $\bar{\sigma}(\Delta)$ making $det\,(I - E\Delta) = 0$.

According to (13),

(1) The magnitude of $\mu(E(s))^{-1}$ is an indicator of the level of interactions, and it corresponds to the impact of interactions on INSYS stability. The smaller the coupling terms in (3) and (4), the smaller E and $\mu(E)$ will be. If $\mu(E(s))^{-1}$ is large enough, the INSYS stability will be ensured for a wide range of controllers that have stabilized the IFSYS.

(2) As $\mu(E(s))^{-1}$ does not depend on the controllers' parameters and only depends on the system parameters and control modes, it can be assumed as the available headroom for the independent design of converters' controllers that stabilize the INSYS. In the case of weak coupling among the converters, $\mu(E(s))^{-1}$ will be sufficiently large, leaving a large headroom for the independent design of controllers that stabilize the INSYS of multiple VSCs.

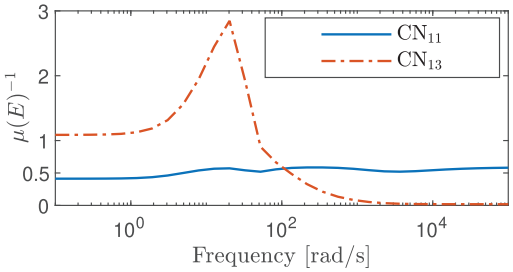

FIGURE 5 $\mu(E(s))^{-1}$ for two control modes versus frequency

It should be noted that the controllers are often designed to provide an acceptable set-point tracking capability for the system. This requirement is usually taken care of by embedding an integrator in the controllers, resulting in $\bar{T} = I$ at low frequencies. Thus, the low-frequency value of $\bar{\sigma}(\bar{T})$ is determined by the controllers' integral action, while the controller order and parameters can be adjusted to shape $\bar{\sigma}(\bar{T})$ in the mid- and high-frequency ranges. As a result, maintaining $\mu(E(s))^{-1} > 1$ at low frequencies is necessary to preserve (13). Satisfying (13) at mid- and high-frequency ranges can be taken care of by the proper selection of controller parameters. Thus, $\mu(E(0))^{-1}$ is an important criterion for the interaction analysis. If $\mu(E(0))^{-1} < 1$ for a certain control mode, any controller with set-point tracking capability would violate (13), and the stability of INSYS cannot be guaranteed even if the IFSYS is stable.

Figure 5 shows two illustrative examples of $\mu(E(s))^{-1}$ for two different sets of control modes, CN_{11} and CN_{13}. To identify which control mode results in larger interactions, firstly, the value of $\mu(E(0))^{-1}$ in the two control modes should be compared to each other. In CN_{13}, $\mu(E(0))^{-1} > 1$, and thus the controller parameters can be selected such that (13) is satisfied and consequently INSYS is stabilized by stabilizing IFSYS. However, in CN_{11}, $\mu(E(0))^{-1} < 1$, which violates (13) for any well-tuned controllers. Therefore, the stabilizing controllers of IFSYS may or may not stabilize the INSYS in CN_{11}. Furthermore, compared to CN_{11}, there is a larger headroom for designing controllers operating in CN_{13} as $\mu(E(s))^{-1}$ is larger, and thus the interactions have less impact on the stability of INSYS in CN_{13}. It should also be noted that although $\mu(E(s))^{-1}$ in CN_{11} is larger than that in CN_{13} for the high-frequency range, the decisive frequency range for the design of controllers such that (13) is satisfied is the low- and mid-frequency ranges. The reason is that by increasing the order of controllers, it would be possible to shape $\bar{\sigma}(\bar{T})$ such that, in the high-frequency range, it approaches zero and consequently satisfies (13).

In Section 5, $\mu(E(s))^{-1}$ will be plotted for all the possible control modes in Table 2, and the impact of the control mode

on the interactions will be investigated accordingly. Prior to the simulations, in the following, it is proved that changing the *d*-axis control mode does not impact $\mu(E(0))^{-1}$.

Proof: Considering the small-signal dynamics of DC-link voltages in Figure 1 and neglecting the DC side perturbations,

$$C_k \frac{\mathrm{d}\tilde{V}_{dc_k}}{\mathrm{d}t} = -\frac{\tilde{P}_k}{V_{dc_{k_0}}} + \frac{P_{k_0}}{V_{dc_{k_0}}^2}\tilde{V}_{dc_k}; \quad k \in \{1,2,3\}. \tag{15}$$

Using (15),

$$\tilde{V}_{dc_k}(s) = \frac{-1}{V_{dc_{k_0}}} \frac{1}{C_k s - \left(\frac{P_{k_0}}{V_{dc_{k_0}}^2}\right)} \tilde{P}_k(s); \quad k \in \{1,2,3\}. \tag{16}$$

Based on (16), when the *d*-axis control mode changes from active power to DC voltage control, the control outputs of the system are related to each other by

$$\underbrace{[\tilde{V}_{dc_1}, y_{q_1}, \tilde{V}_{dc_2}, y_{q_2}, \tilde{V}_{dc_3}, y_{q_3}]^T}_{y_{dc}} = W(s) \underbrace{[\tilde{P}_1, y_{q_1}, \tilde{P}_2, y_{q_2}, \tilde{P}_3, y_{q_3}]^T}_{y_P}, \tag{17}$$

where

$$W(s) = diag\left\{\left[\frac{-1}{V_{dc_{k_0}}\left(C_k s - \left(\frac{P_{k_0}}{V_{dc_{k_0}}^2}\right)\right)}, 1\right]\right\}. \tag{18}$$

Assuming $P_{k_0} = 1$ [p.u.] and $V_{dc_{k_0}} = 1$ [p.u.], it can be derived that $W(0) = I$ and consequently, $\mu(E(0))^{-1}|_{y_{dc}} = \mu(E(0))^{-1}|_{y_P}$. Therefore, if $\mu(E(0))^{-1} > 1$ is satisfied for the DC voltage control mode, it will also be satisfied for the active power control mode.

4 | VSCs CONTROL DESIGN FOR INTERACTION MITIGATION

In this section, a criterion is proposed for designing the controllers of the IFSYS independently, which ensures INSYS stability as well. The main advantage of the proposed controller design is the mitigation of the negative impact of interactions on the interconnected system stability. It should be noted that this procedure can be applied to any type of individual controller as it aims at re-tuning the individual controllers to mitigate the interactions. For example, if robust controllers are initially designed for the individual converters, the proposed procedure can be utilized to design a set of robust controllers that ensure the stability of INSYS.

With an integrator in the outer control loops to achieve set-point tracking capability, $\mu(E(0))^{-1} > 1$ will become a necessary condition for using (13) to design the controllers of the IFSYS such that INSYS stability is ensured. The main steps for designing the controllers for each VSC are as follows:

(1) Set the time constant of the inner controller (τ) and find the inner controller parameters as explained in [11]. Find $K_k^{in,cl}(s)$ in (9) and determine $\bar{G}_{kk}(s)K_k^{in,cl}(s)$.
(2) Decide on the bandwidth of the outer control loop (BW_o) by considering the rule of thumb for cascaded inner-outer loops as $BW_o < \frac{0.1}{\tau}$. Depending on the order of $\bar{G}_{kk}(s)$, choose the order of the outer controller $K_k^o(s)$. An integral action must be included in the outer controller. Knowing $\bar{G}_{kk}(s)K_k^{in,cl}(s)$, $K_k^o(s)$ is the only unknown in the control structure of Figure 3a. Tune the parameters of $K_k^o(s)$ to create a stable feedback loop in Figure 3a and ensure the desirable time-domain specifications.
(3) Check whether (13) is satisfied. Depending on the magnitude of $\mu(E(s))^{-1}$, there will be an available headroom for the design of controllers.
(4) If (13) is satisfied, the design is complete. Otherwise, change the parameters of the outer controllers in step 2 and repeat steps 2–4.

In cases where $\mu(E(0))^{-1} < 1$, a joint controller design for VSCs (in contrast to an independent design) may result in satisfying (13) and thus reducing the negative impact of interactions on stability. In the joint design, the coupling among certain converters is taken into account in the control design. To perform the joint control design, $\bar{G}(s)$ in (8) is modified after the dynamics of the converters forming a group are moved from the *coupling* term to the *uncoupled dynamics* term in (3) and (4). As an example, to perform the joint design for VSC_1 and VSC_2, while designing VSC_3 independently, $\bar{G}(s)$ is defined as,

$$\bar{G}(s) = \begin{bmatrix} \bar{G}_{11}(s) & \bar{G}_{12}(s) & 0 \\ \bar{G}_{21}(s) & \bar{G}_{22}(s) & 0 \\ 0 & 0 & \bar{G}_{33}(s) \end{bmatrix}. \tag{19}$$

The converters involved in the joint design are mainly those manufactured by a single vendor as this will ensure access to the detailed model of those converters. The proposed control design will facilitate the multi-vendor realization of hybrid AC/DC systems as it will ensure design confidentiality by joint design of converters' controllers whose models are available and independent control design of converters whose models are confidential [22, 23].

In Section 5, certain recommendations will be given about the control mode of the converters included in the joint control design to reduce the impact of interactions on the interconnected system stability. These recommendations will be based on the magnitude of $\mu(E(s))^{-1}$ for various control modes of the converters forming a group.

5 | CASE STUDY

In this section, the impact of control modes on the interactions and the viability of the proposed stability criterion for the controller design is studied using a test system with three converters sharing a PCC with the parameters given in

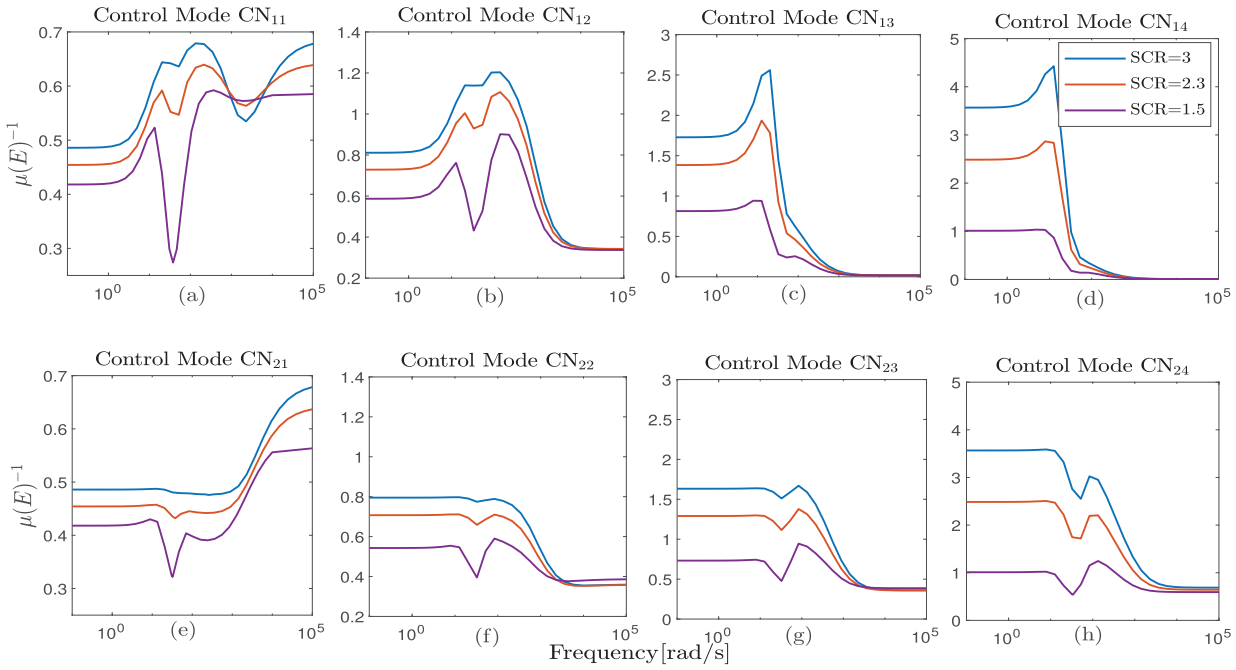

FIGURE 6 $\mu(E)^{-1}$ against frequency for various sets of control modes in Table 2 and for several SCRs, $P_1 = P_2 = P_3 = 1$ [p.u.]

Table 1. This study covers the range of SCRs from strong (SCR> 3) to weak (2 < SCR < 3) and very weak AC systems (SCR< 2) [24]. The nonlinear model of the test system is built in MATLAB/SIMULINK, and the linearized system is obtained to form the small-signal model required for the aforementioned studies.

5.1 | Impact of converters' control modes on interactions

To evaluate the impact of control modes on the level of interactions among converters, $\mu(E(s))^{-1}$ for various SCR values and the control modes of Table 2 is depicted in Figure 6. In Figure 6, the sub-figures next to each other have the same *d*-axis control mode, and the ones on the top and bottom rows have the same *q*-axis control mode.

To investigate the impact of the *q*-axis control mode on the interactions, Figure 6a–d shows $\mu(E(s))^{-1}$ for various sets of *q*-axis control modes and a fixed *d*-axis control mode (DC voltage control mode). In Figure 6a,b, $\mu(E(0))^{-1} < 1$, which violates (13) for any well-tuned controller, and thus the INSYS stability is not guaranteed even if IFSYS is stable. However, in Figure 6c,d, $\mu(E(0))^{-1} > 1$ for several SCR values. Therefore, the controller parameters of the IFSYS in control modes CN_{13} and CN_{14} can be set based on the step-by-step procedure discussed in Section 3. C to satisfy (13) and consequently stabilize the INSYS. Additionally, for all SCRs, $\mu(E(s))^{-1}$ is larger in Figure 6d than that of Figure 6c for the low- and mid-frequency ranges, which results in a larger available headroom for designing the converters' controllers in control mode CN_{14}. Similar conclusions can be made about the impact of *q*-axis control mode on the interactions based on Figure 6e–h.

To study the impact of *d*-axis control mode on the interactions, each of Figure 6a–d are compared with their counterparts in Figure 6e–h, with the same *q*-axis control mode and a different *d*-axis control mode. It is observed that the *d*-axis control mode does not impact $\mu(E(0))^{-1}$, which was also proved in Section 3. This means that, in the proposed control design based on (13), the *d*-axis control mode does not affect the relationship between the IFSYS and INSYS stability.

In summary, when all the VSCs operate in AC voltage control mode, the largest interactions happen (Figure 6a,e). Moving from Figure 6a(e) toward Figure 6d(h) with more VSCs in the reactive power control mode will reduce the impact of interactions on the stability of INSYS, regardless of the *d*-axis control mode. However, the control design headroom in the DC voltage control mode is larger than that in the active power control mode as $\mu(E(s))^{-1}$ is larger, Figure 6.

Figure 7 shows $\mu(E(s))^{-1}$ and $\bar{\sigma}(\bar{T})$ for DC voltage control mode and various sets of *q*-axis control mode. It should be noted that Figure 7 is plotted for a certain set of controller parameters for illustration purposes only. As Figure 7 shows, the only control mode for which (13) is satisfied and thus for which the independent design of the converters has stabilized the INSYS is control mode CN_{14}, where all the converters control the reactive power. In this control mode, the set-point tracking capability as well as stability is ensured for the INSYS by the independent control design of the IFSYS. In other control modes in Figure 7a–c, while the order of the controller can adjust the high-frequency characteristics of $\bar{\sigma}(\bar{T})$, the low-frequency characteristics of $\bar{\sigma}(\bar{T})$ mainly depends on the integral action. Since $\mu(E(0))^{-1} < 1$ in Figure 7a–c, $\bar{\sigma}(\bar{T}) < \mu(E(s))^{-1}$ cannot be achieved and the stability of the INSYS cannot be guaranteed. The eigenvalue map of the system for each control mode verifies the

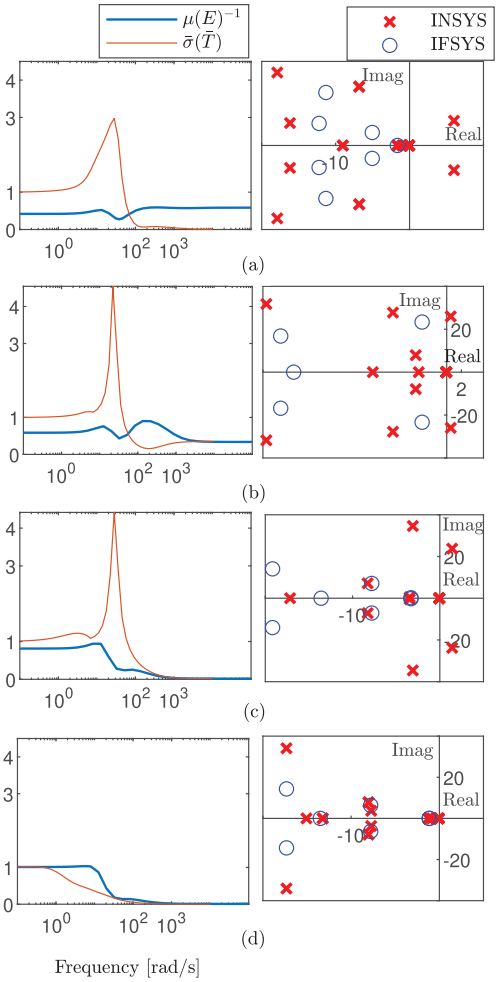

FIGURE 7 $\bar{\sigma}(\bar{T})$, $\mu(E)^{-1}$ and eigenvalue plot of IFSYS and INSYS for (a) control mode CN_{11}, (c,d) control mode CN_{12}, (c) control mode CN_{13}, and (d) control mode CN_{14}, SCR=1.5

INSYS stability in control mode CN_{14}, which is shown in Figure 7.

5.2 | Impact of converters' joint control design on interactions

For the set of control modes discussed in Table 2, various scenarios of joint design can be considered. For example, in control mode CN_{12}, the first scenario would consider the two VSCs in the AC voltage control mode as a group (VSC_1 and VSC_2), and the third VSC in the reactive power control mode as an independent unit (VSC_3). The second scenario is to form a group consisting of one of the converters in AC voltage control mode and one in reactive power control mode ((VSC_1 or VSC_2) and VSC_3) for the joint design, while designing the controller of the other VSC in AC voltage control mode independently (VSC_2 or VSC_1). For control mode CN_{11} in Table 2, since all the VSCs have similar parameters and ratings, there is only one joint design scenario, where any of the two VSCs are involved in the joint design, and the third VSC is considered as an independent unit. The rest of the possible joint design scenarios can be obtained similarly.

Figure 8 shows $\mu(E(s))^{-1}$ when VSC_2 controller is designed as an independent unit, and VSC_1 and VSC_3 form a group and their controllers are jointly designed. By comparing Figure 8 against Figure 6 in each control mode, it can be observed that due to the joint control design, all $\mu(E(s))^{-1}$ curves have shifted up, indicating that the available headroom for designing stabilizing controllers has become larger, and the interactions have decreased. However, even with the joint control design, in control modes CN_{11} and CN_{21}, $\mu(E(0))^{-1} < 1$ and thus, (13) cannot be satisfied for any controller with an integral action, Figure 8a,e. Also, there is not any other distinct joint design scenario that would result in $\mu(E(0))^{-1} > 1$. Thus, having all the VSCs in AC voltage control mode results in the highest interaction level among the VSCs, and the joint design will not be a remedial action in this case to make $\mu(E(0))^{-1} > 1$ and consequently the INSYS stability cannot be guaranteed.

Another scenario is the joint design of VSC_1 and VSC_2 in control modes CN_{12} and CN_{22}, where the converters operating in AC voltage control mode form a group, and the converter in reactive power control mode is considered as an individual unit. For this scenario, $\mu(E(s))^{-1}$ is shown in Figures 9a and c. Comparing $\mu(E(s))^{-1}$ in Figures 9a and c with Figures 8b and f reveal that this joint design scenario results in a larger $\mu(E(s))^{-1}$. Especially, $\mu(E(0))^{-1} > 1$ in Figure 9a,c indicating that (13) can be met and the INSYS can be stabilized by stabilizing the IFSYS.

In control modes CN_{13} and CN_{23}, the joint control design of VSC_2 and VSC_3 results in another feasible scenario, where the controllers of VSCs operating in reactive power control mode are jointly designed, and the controller of the VSC in AC voltage control mode is designed independently. Comparing $\mu(E(s))^{-1}$ in Figure 9b,d against Figure 8c,g shows that a smaller $\mu(E)^{-1}$, and thus, a smaller stability headroom is provided with the joint design of the VSCs when the VSC in the AC voltage control mode is designed independently.

Based on Figures 6, 8 and 9, it can be concluded that

(1) Joint design of VSCs's controllers can always lessen the impact of interactions on the interconnected system stability as $\mu(E(s))^{-1}$ curves have shifted up in Figures 8 and 9 compared to Figure 6.
(2) Joint control design of converters operating in AC voltage control mode, such that no converter in AC voltage control mode is designed individually, corresponds to the recommended design scenario in terms of interaction mitigation. However, when all converters operate in AC voltage control mode, the joint design might not necessarily reduce the high level of interactions and may not ensure the INSYS's stability.
(3) If for any operational reasons, it is not possible to jointly design the converters in AC voltage control mode, it is recommended to form the groups of the converters such that the lowest number of converters in AC voltage control mode is designed independently.

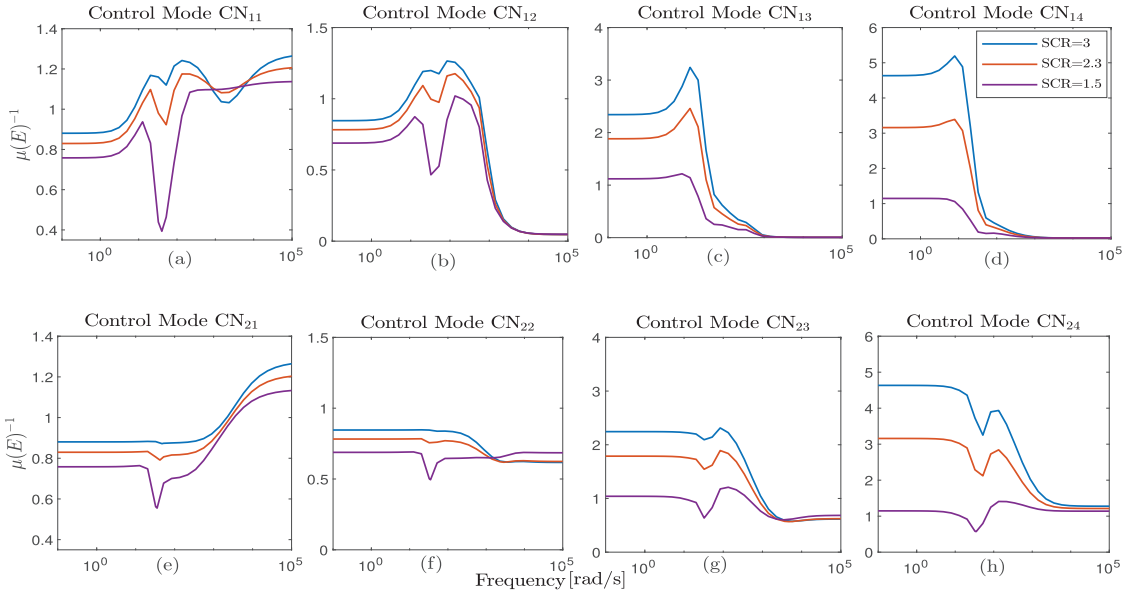

FIGURE 8 $\mu(E(s))^{-1}$ against the frequency for various sets of control modes in Table 2 with VSC_1 and VSC_3 forming a group

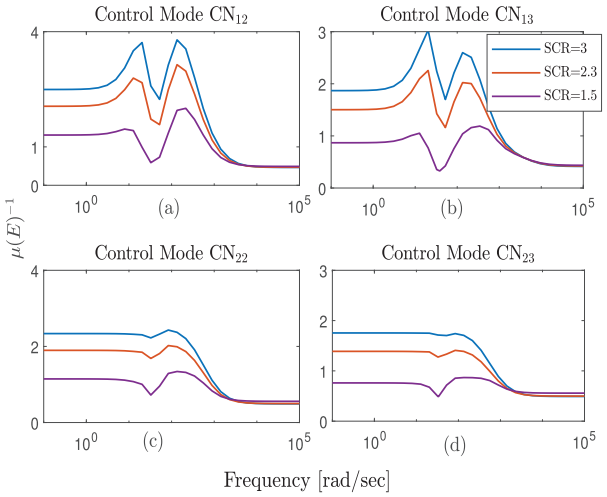

FIGURE 9 $\mu(E)^{-1}$ against frequency for various SCRs with joint design for (a,c) VSC_1 and VSC_2, and (b,d) VSC_2 and VSC_3

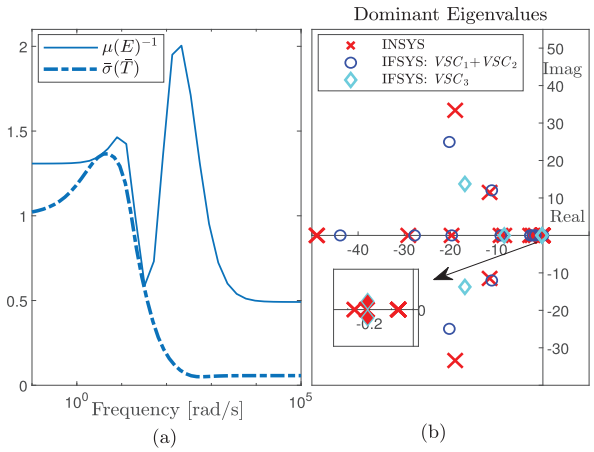

FIGURE 10 $\bar{\sigma}(\bar{T})$, $\mu(E)^{-1}$ and eigenvalue plot of IFSYS and INSYS for the joint design of VSC_1 and VSC_2 in control mode CN_{12}

5.3 | Joint design of stabilizing controllers

5.3.1 | Joint design of VSC_1 and VSC_2 in control mode CN_{12}

As an example to clarify the impact of controllers' joint design on the external control loop interactions, control mode CN_{12} is considered with the 3-VSC system operating under SCR = 1.5. As shown in Figures 6 and 9, CN_{12} is the control mode with the highest interaction level for which the controllers can be designed independently to satisfy (13) and consequently to ensure the stability of the INSYS. It should be noted that for CN_{11}, stabilizing controllers cannot be designed based on (13). It is assumed that VSC_1 and VSC_2, operating in AC voltage control mode, are built by the same manufacturer, and thus their joint controller design is possible. Figure 10 shows $\mu(E(s))^{-1}$ and $\bar{\sigma}(\bar{T})$ for the controllers designed based on steps 1–4 of the control design procedure in Section 3. C for VSC_1 and VSC_2 as a group and for VSC_3 as an individual unit. As the sufficient condition (13) is satisfied according to Figure 10, it is guaranteed that the INSYS of three VSCs is stable even in the presence of interactions. The eigenvalue map of the INSYS of three VSCs is also shown in Figure 10, which confirms that the INSYS is stable.

5.3.2 | Joint design of VSC_1 and VSC_3 in control mode CN_{13}

In control mode CN_{13}, when the 3-VSC system operates under SCR = 1.5, the joint control design of the VSC controlling the AC voltage (VSC_1) and the VSC controlling the reactive

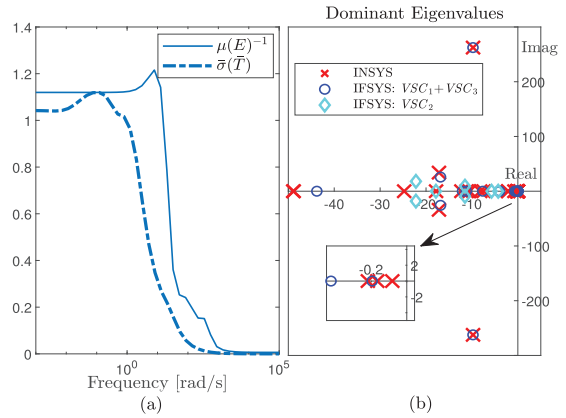

FIGURE 11 $\bar{\sigma}(\bar{T})$, $\mu(E)^{-1}$ and eigenvalue plot of IFSYS and INSYS for the joint design of VSC_1 and VSC_3 in control mode CN_{13}

power (VSC_3) is a remedial action to reduce the interactions. Based on the procedure discussed in Section 4, Figure 11 shows $\mu(E(s))^{-1}$ and $\bar{\sigma}(\bar{T})$ for the designed controllers. As shown in Figure 11, the sufficient condition (13) is satisfied in this control design, and therefore, it is guaranteed that the INSYS of three VSCs is stable even in the presence of interactions. Figure 11 shows the eigenvalue map confirming that the INSYS is stable.

6 | CONCLUSION

In this paper, external control loop interactions among VSCs sharing a common AC system were studied, and the impact of control mode on the interactions was investigated. μ analysis was used to measure the level of interactions for various sets of control modes and identify the set of control modes for which the stability of individual VSCs can ensure the stability of the interconnected system (INSYS) of VSCs. The analysis indicated that, regardless of the *d*-axis control mode, the largest interactions occur if the adjacent converters simultaneously regulate the AC voltage via their *q*-axis control loop. Furthermore, having more VSCs in the reactive power control mode will lessen the impact of interactions on stability. Moreover, there is a larger headroom for the independent design of stabilizing converters' controllers in the DC voltage control mode than in the active power control mode.

A sufficient stability criterion was also proposed for the independent design of converters' outer control loops such that the multi-VSC system stability is ensured. In case of severe interactions, where the INSYS becomes unstable even if each VSC is stable, a joint control design was proposed to stabilize the INSYS. The performed stability analysis illustrated that the joint control design of converters in AC voltage control mode such that the lowest number of converters in AC voltage control mode are designed independently is the best remedial action to reduce the impact of control loop interactions on the stability of multi-VSC systems.

CONFLICT OF INTEREST

The authors declare no conflict of interest.

DATA AVAILABILITY STATEMENT

Data sharing not applicable to this article as no datasets were generated or analysed during the current study.

ORCID

Fatemeh Ahmadloo https://orcid.org/0000-0001-7291-0300
Sahar Pirooz Azad https://orcid.org/0000-0002-6194-4182

REFERENCES

1. Huang, Y., Wang, D., Shang, L., Zhu, G., Tang, H., Li, Y.: Modeling and stability analysis of DC-link voltage control in multi-VSCS with integrated to weak grid. IEEE Trans. Energy Convers. 32(3), 1127–1138 (2017)
2. Wan, C., Huang, M., Chi, K.T., Ruan, X.: Effects of interaction of power converters coupled via power grid: A design-oriented study. IEEE Trans. Power Electron. 30(7), 3589–3600 (2014)
3. Zhou, J.Z., Gole, A.M.: VSC transmission limitations imposed by ac system strength and AC impedance characteristics. In: 10th IET International Conference on AC and DC Power Transmission (ACDC 2012), pp. 1–6. IEEE, Piscataway, NJ (2012)
4. Cole, S., Belmans, R.: A proposal for standard VSC HVDC dynamic models in power system stability studies. Electr. Power Syst. Res. 81(4), 967–973 (2011)
5. Huang, Y., Yuan, X., Hu, J., Zhou, P.: Modeling of VSC connected to weak grid for stability analysis of DC-link voltage control. IEEE J. Emerging Sel. Top. Power Electron. 3(4), 1193–1204 (2015)
6. Huang, Y., Wang, D.: Effect of control-loops interactions on power stability limits of VSC integrated to AC system. IEEE Trans. Power Delivery 33(1), 301–310 (2017)
7. Zhou, P., Yuan, X., Hu, J., Huang, Y.: Stability of DC-link voltage as affected by phase locked loop in VSC when attached to weak grid. In: 2014 IEEE PES General Meeting | Conference and Exposition, pp. 1–5. IEEE, Piscataway, NJ (2014)
8. Wang, D., Hou, Y., Hu, J.: Effect of AC voltage control on the stability of weak AC grid connected DFIG system. In: 2016 IEEE PES Asia-Pacific Power and Energy Engineering Conference (APPEEC), pp. 1528–1533. IEEE, Piscataway, NJ (2016)
9. Yuan, H., Yuan, X., Hu, J.: Modeling of grid-connected VSCS for power system small-signal stability analysis in DC-link voltage control timescale. IEEE Trans. Power Syst. 32(5), 3981–3991 (2017)
10. Huang, Y., Yuan, X., Hu, J., Zhou, P., Wang, D.: DC-bus voltage control stability affected by AC-bus voltage control in VSCS connected to weak AC grids. IEEE Trans. Emerging Sel. Top. Power Electron. 4(2), 445–458 (2015)
11. Yazdani, A., Iravani, R.: Voltage-Sourced Converters in Power Systems: Modeling, Control, and Applications. John Wiley & Sons, Hoboken, NJ (2010)
12. Shen, L., Barnes, M., Milanovic, J.V., Bell, K.R., Belivanis, M.: Potential interactions between VSC HVDC and STATCOM. In: 2014 Power Systems Computation Conference, pp. 1–7. IEEE, , Piscataway, NJ (2014)
13. Rosso, R., Andresen, M., Engelken, S., Liserre, M.: Analysis of the interaction among power converters through their synchronization mechanism. IEEE Trans. Power Electron. 34(12), 12321–12332 (2019)
14. Rosso, R., Buticchi, G., Liserre, M., Zou, Z., Engelken, S.: Stability analysis of synchronization of parallel power converters. In: IECON 2017-43rd Annual Conference of the IEEE Industrial Electronics Society, pp. 440–445. IEEE, Piscataway, NJ (2017)
15. Rosso, R., Engelken, S., Liserre, M.: Robust stability investigation of the interactions among grid-forming and grid-following converters. IEEE Trans. Emerging Sel. Top. Power Electron. 8(2), 991–1003 (2019)
16. Rosso, R., Engelken, S., Liserre, M.: Analysis of the parallel operation between synchronverters and pll-based converters. In: 2019 IEEE Energy Conversion Congress and Exposition (ECCE), pp. 2583–2590. IEEE, Piscataway, NJ (2019)
17. Wang, D., Zhang, X., Yang, L., Huang, Y., Huang, W., Wu, C., Li, S.: Analysis of synchronization stability for multi VSCS parallel-connected to weak grids by improved net damping criterion. Energies 13(13), 3316 (2020)

18. Agbemuko, A.J., Domínguez García, J.L., Prieto Araujo, E., Gomis Bellmunt, O.: Advanced impedance-based control design for decoupling multi-vendor converter HVDC grids. IEEE Trans. Power Delivery 35(5), 2459–2470 (2020)
19. Ahmadloo, F., Pirooz Azad, S.: The impact of control modes on the external control loop interactions in VSC-HVDC systems. In: 2021 IEEE Power & Energy Society General Meeting (PESGM), pp. 1–5. IEEE, Piscataway, NJ (2021)
20. 3-Terminal HVDC Link with 2-Level VSC Terminals. https://www.pscad.com/knowledge-base/article/191. Accessed Janurary, 12, 2023
21. Skogestad, S., Postlethwaite, I.: Multivariable Feedback Control: Analysis and Design. vol. 2. Wiley, New York (2007)
22. Despouys, O., Rault, P., Burgos, A., Vozikis, D., Guillaud, X., Larsson, T.: Assessment of interoperability in multi-vendor VSC-HVDC systems: Interim results of the best paths demo# 2. In: 2018 CIGRE Session. CIGRE, FRA (2018)
23. Chaffey, G., Rahman, M.H., Page, F., Jahn, I., Ponnalagan, B., Ishida, K., Kunjumuhammed, L., Wang, M., Hertem, D.V., Cowan, I.: Demonstration of multi-vendor protection systems for multiterminal vsc-hvdc networks. In: 2021 IEEE Madrid PowerTech, pp. 1–6. IEEE, Piscataway, NJ (2021)
24. Group, I.W., et al. IEEE guide for planning dc links terminating at ac locations having low short-circuit capacities. IEEE, Piscataway, NJ (1997)

How to cite this article: Ahmadloo, F., Pirooz Azad, S.: Grid interaction of multi-VSC systems for renewable energy integration. IET Renew. Power Gener. 17, 1212–1223 (2023). https://doi.org/10.1049/rpg2.12676

APPENDIX

Derivation of (9): Considering the cascaded control scheme

$$u_{d,q_k} = K_k^{in}(s)(i_{d,q_k}{}^{*} - i_{d,q_k}). \tag{A.1}$$

Using the the inner decoupling filters [11], the current dynamics at the AC side is given by

$$L_{f_k}\dot{i}_{d,q_k} = -R_{f_k} i_{d,q_k} + u_{d,q_k}. \tag{A.2}$$

Thus,

$$i_{d,q_k}(s) = \frac{u_{d,q_k}(s)}{L_{f_k}s + R_{f_k}}. \tag{A.3}$$

Substituting (A.3) in (A.1), results in

$$K_k^{in,cl}(s) = \frac{u_{d,q_k}(s)}{i_{d,q_k}{}^{*}} = \frac{K_k^{in}(s)}{1 + K_k^{in}(s)\left(\frac{1}{L_{f_k}s+R_{f_k}}\right)}. \tag{A.4}$$

The inner–outer controller then is given by $K_k(s) = K_k^{in,cl}(s)K_k^{o}(s)$.